Optically detected electron paramagnetic resonance of AlN single crystals

P. M. Mason,* H. Przybylinska,† and G. D. Watkins
Department of Physics, Lehigh University, Bethlehem, Pennsylvania 18015

W. J. Choyke
Department of Physics, University of Pittsburgh, Pittsburgh, Pennsylvania 15620

G. A. Slack
Department of Physics, Rensselaer Polytechnic Institute, Troy, New York 12180
(Received 7 August 1998)

AlN single crystals have been investigated using photoluminescence (PL) and optical detection of electron paramagnetic resonance in the PL (ODEPR). All crystals were found to exhibit intense PL extending from the visible into the near infrared. Several $S=1$ centers, each with its own distinct emission spectrum, and distant $S=1/2$ pair recombination centers have been observed via ODEPR. In all except one center, $D5$, no hyperfine structure was observed preventing chemical identification of the impurity involved. In the case of $D5$ the partially resolved hyperfine structure suggests interaction with a 100% abundant nucleus of $I\sim 5/2$. We present arguments to associate it with a displaced host aluminum atom. [S0163-1829(99)03004-0]

I. INTRODUCTION

AlN is receiving increasing attention for use in visible and UV optoelectronic $Al_xGa_{1-x}N$ alloy devices, as well as for high-temperature electronic applications, high thermal conductivity films, and potentially radiation hardened materials.[1–4] As far as its defects are concerned, AlN is known to have a high affinity for oxygen. Various studies including thermal conductivity,[5] luminescence,[6,7] optical absorption, and electron paramagnetic resonance[8] (EPR) measurements have been performed to characterize the oxygen content. Early studies identified visible luminescence bands resulting from doping AlN powder with Mn,[9] and the rare earths Sm and Eu.[10] More recent studies have identified several sharp near-infrared zero-phonon luminescence lines with additional specific $3d$ transition element impurities,[11–14] taking advantage of their close similarity to lines that had previously been studied in more detail in GaN.[11,12,15–17]

In addition, an EPR and optical absorption study in neutron-irradiated polycrystalline material has correlated an absorption band at 370 nm with an EPR signal at $g=2.007$.[18,19] The defect responsible was tentatively assigned to the N vacancy (V_N). Theoretical studies predict V_N to have a deep donor level between 0.7 eV and 0.9 eV below the conduction-band edge, in contrast to V_N in GaN, which is calculated to be a shallow donor.[20–22] Oxygen has also been predicted to have a deep donor level.[23] However, very few experimental structural studies of point defects in AlN have been published.

In the present study single-crystal AlN samples have been examined using the techniques of photoluminescence (PL) and optical detection of EPR in the PL (PL-ODEPR) to probe for defects. This is the first known study of AlN using ODEPR, and the focus of the investigation is on the as-grown impurities and defects present in the samples.

II. EXPERIMENTAL PROCEDURE

Single-crystal samples from three different sources were studied. One set, supplied by one of the authors (W.J.C.), were small hexagonal crystallites, $\sim(0.5\ \text{mm})^3$, grown at Westinghouse Research Laboratory (WRL) by R.B. Campbell in the 1960s using a high-temperature Lely vapor-transport technique from ALCOA grade AlN powder in a graphite furnace.[24] Their crystal morphology exhibited a long axis (the [0001] c axis) with a uniform hexagonal cross section formed by $\{1\bar{1}00\}$ surfaces, in analogy to SiC.[25] (This will be established in the next section from the ODEPR results.) The samples were transparent, with a slight grayish-green tint. In addition to substantial concentrations of O and C, possible contaminants have been suggested to include B, Ti, V, and Cr, most of which presumably emanated from the graphite furnace. A second pair of samples, supplied by another of the authors (G.A.S.), had been cut from a single crystal boule grown in the 1970s at General Electric Research Laboratory (GERL). In this case, a two-step purification procedure was used, followed by vapor transport single-crystal growth in a sealed tungsten crucible.[26] These larger samples were amber colored, with approximate dimensions $\sim 1\times 1\times 3$ mm, with the c axis oriented along the long dimension. One of them, W-154, had previously been characterized by thermal conductivity and optical measurements to be of high chemical purity.[26] For it, the oxygen content can be estimated to be only ~ 400 ppm by weight ($\sim 5\times 10^{19}\ \text{cm}^{-3}$), by comparison of its thermal conductivity and optical absorption data to that of another high purity sample, W201, for which the oxygen concentration was directly measured.[5] For the GERL samples, the carbon content should also be low, being grown in a tungsten rather than a graphite furnace. A third sample had been grown also in the 1970s by A. Armington at Air Force Cambridge Research Laboratory (AFCRL) in a carbon crucible. It was dark green in color, and by characterization of its optical absorption, it had previously been determined to be of lower purity, with strong oxygen-related UV absorption and a band in the visible spectrum tentatively attributed to carbon.[26]

In the PL and PLODEPR experiments, excitation was supplied by the 351, 364, 458, 476, 488, or 514 nm lines of

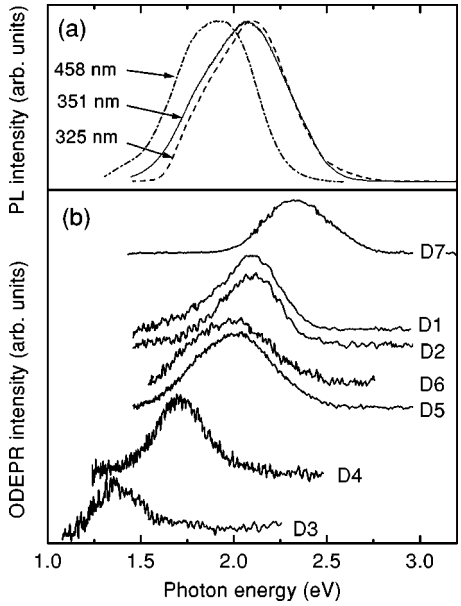

FIG. 1. (a) Photoluminescence of a WRL AlN single crystal under excitation at three different laser wavelengths, as indicated. (b) Spectral dependencies of seven different ODEPR resonances, taken under 351-nm ($D1$,$D2$), 458-nm ($D3$-$D6$), and 325-nm ($D7$) excitation. All curves have been normalized to have comparable peak intensities. The corresponding ODEPR spectra are shown in Fig. 2.

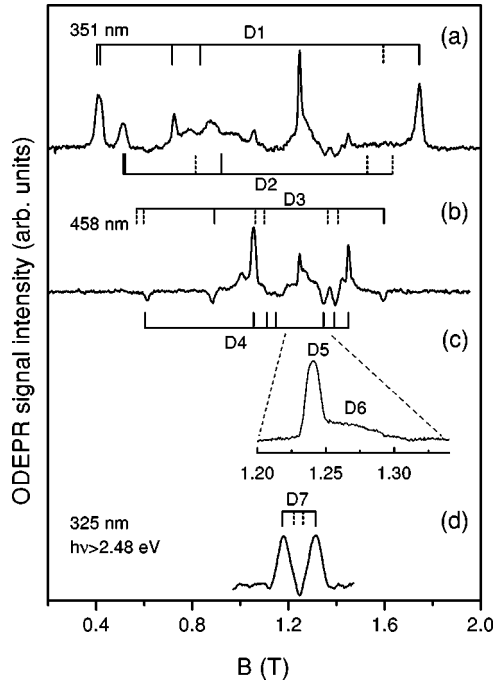

FIG. 2. ODEPR spectra in WRL AlN under 351 nm (a), 458 nm (b,c) and 325 nm (d) excitation for $\mathbf{B}\|[1\bar{1}00]$. In (c) the magnetic field has been expanded to show signals near $g=2$. In (d) a 2.48-eV high energy pass filter was used in order to supress other centers. The observed resonance transitions for each center are indicated with solid lines, those with negligible intensity are marked by dashed lines.

an Ar^+ ion laser, the 325 nm line of a He-Cd laser, or the 244 nm line of a CW frequency-doubled Ar^+ ion laser, all below the AlN band gap of 6.3 eV. The excitation intensity employed ranged from 0.1 to 60 mW/mm^2, depending upon excitation wavelength and the sample studied.

The PL and PL-ODEPR were performed at pumped liquid He temperatures ($\sim$1.7 K) in a 35-GHz spectrometer which has been previously described.[27] The PL was collected along the magnetic-field direction, and detected by a silicon diode (EGG HUV2000B). Excitation was perpendicular to the magnetic field, unless stated otherwise. The spectral dependence of an ODEPR signal was determined by inserting a monochromator before the detector and monitoring its strength as the monochromator was scanned. Polarization studies of the PL from the individual and differently oriented defects were performed by monitoring the strength of their corresponding ODEPR signals vs polarization axis orientation of a polaroid filter placed before the detector. For polarization studies while using the monochromator, a second polaroid was placed immediately before the monochromator with its polarization axis oriented at 45° relative to the ruling of its grating, to avoid polarization effects of the grating itself. Electron irradiation of a few of the samples was performed at room temperature using a 2.5-MeV Van de Graaff accelerator, with doses varying from 0.5 to 2.5×10^{18} cm^{-2}.

III. EXPERIMENTAL RESULTS

Consider first the WRL samples. These samples all exhibit strong PL extending from the visible into the near infrared, with a broad peak position shifting towards lower energy for lower excitation wavelengths. Shown in Fig. 1(a) are typical PL spectra detected for three different excitation wavelengths for one of the samples. Using a variety of photoexcitation energies and intensities, in addition to microwave amplitude modulation frequencies and magnetic-field orientations, it was possible to extract at least seven distinct ODEPR signals associated with different centers contributing to the luminescence. A measurement of the spectral dependence of each ODEPR signal allowed its luminescence band to be extracted from the total spectra, and is shown in Fig. 1(b). The luminescence is therefore made up of many broad overlapping bands, none of which appear to correlate with bands previously reported in the literature. In Fig. 2, we show the individual ODEPR spectra for $\mathbf{B}\|[1\bar{1}00]$, as partially separated by different excitation energies and appropriate filters.

In the AFCRL sample, $D1$, $D2$, $D5$, and a particularly strong $D7$ were detected, plus many additional ODEPR signals originating from PL in the near infrared. These additional signals will not be treated here.

In the GERL samples, similar, but an order of magnitude less intense, PL was observed, but shifted slightly to lower energy, as shown in Fig. 3(a). Remarkably, none of the prominent ODMR signals seen in the WRL and AFCRL samples were observed. Instead, five new ODEPR signals were observed, the spectral dependencies of which are shown in Fig. 3(b). In Fig. 4, we show the individual spectra, partially separated under different excitation conditions, for $\mathbf{B}\|[11\bar{2}0]$.

For all samples, 244-nm excitation appeared to produce the same PL-ODEPR signals, with no new ones. The

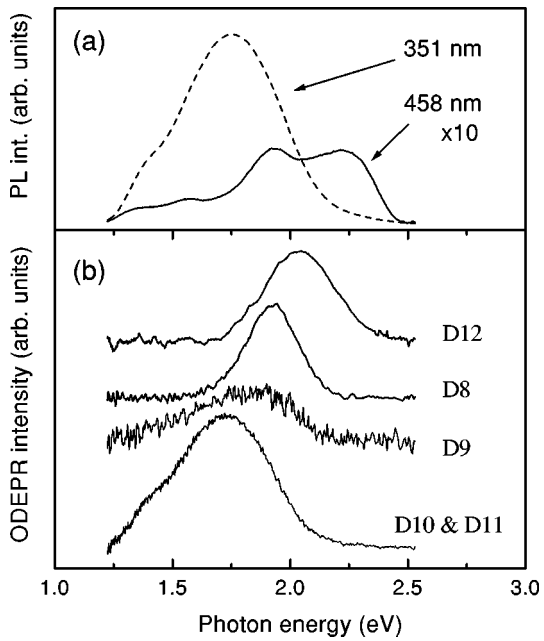

FIG. 3. (a) Photoluminescence of a GERL AlN sample (W154) under excitation at 351- and 458-nm laser wavelengths. Note the decrease in PL intensity for longer-wavelength excitation. (b) Spectral dependencies of five ODEPR signals taken under 458-nm ($D8$) and 351-nm ($D9$-$D12$) excitation.

ODEPR signal-to-noise was substantially reduced, however, due to the higher noise level associated with the frequency doubled laser source, and was therefore not used for the detailed PL-ODEPR studies. Similarly, the He-Cd laser 325-nm excitation was used only where necessary to produce a specific defect luminescence, being substantially noisier than the Ar^+ ion laser lines. In what follows, we will describe the principal spectroscopic features of each of the spectra separately.

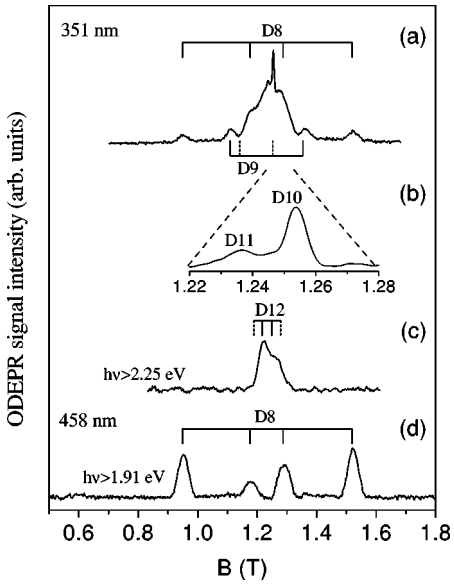

FIG. 4. ODEPR spectra of the W154 sample recorded under excitation with 351-nm (a,b,c) and 458-nm (d) Ar ion laser lines for $\mathbf{B}\|[11\bar{2}0]$. In (b) the magnetic field has been expanded to show resonances near $g=2$. The spectra shown in (c) and (d) have been taken using high-energy pass filters, as indicated in the figure.

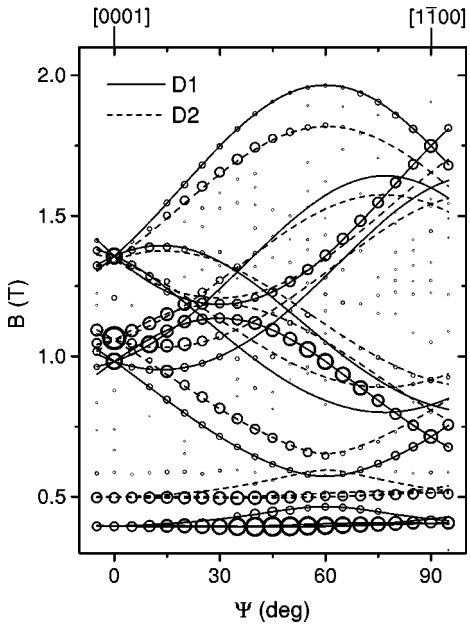

FIG. 5. Angular dependencies of $D1$ and $D2$ ODEPR signals for **B** rotated in the $(11\bar{2}0)$ plane. The areas of the circles are proportional to the experimental ODEPR intensities. The solid ($D1$) and dashed ($D2$) lines are theoretical fits to the data using Eq. (1) and the parameters given in Table I.

A. $D1$ and $D2$

As shown in Fig. 2(a), there are two dominant ODEPR spectra seen under 351-nm (or 364-nm) excitation, which we label $D1$ and $D2$. They are absent for the longer available excitation wavelengths. Both $D1$ and $D2$ were observed in all seven of the WRL samples surveyed, as well as the one from AFCRL. Their signals are all positive (increase in PL intensity at resonance) and their spectral dependencies, shown in Fig. 1(b), appear identical.

Shown in Fig. 5 is the angular dependence of their ODEPR signals detected using 351-nm excitation for the magnetic field **B** rotating in the $(11\bar{2}0)$ crystal plane. The solid lines are theoretical least squares fits to the data using the conventional spin Hamiltonian:

$$\mathcal{H}=\mu_B\mathbf{S}\cdot\mathbf{g}\cdot\mathbf{B}+\mathbf{S}\cdot\mathbf{D}\cdot\mathbf{S}, \tag{1}$$

for an electronic spin, $S=1$. Here μ_B is the Bohr magneton, and **D**, the fine-structure tensor. The lines that are mirrored in their angular dependencies about $g=2$ are the ''$\Delta M_S=\pm 1$'' transitions. The low-field lines with weak angular dependencies are ''$\Delta M_S=\pm 2$'' transitions. The quotation marks are used because the fine-structure interaction energy is on the order of the microwave energy and strong mixing of the M_S states occurs. Evidence of this is the strong intensity of the ''unallowed'' $\Delta M_S=\pm 2$ transitions.

Combining these results with similar detailed studies in the $(1\bar{1}00)$ plane, not shown, the spin Hamiltonian parameters given in Table I were determined, providing the excellent fits shown in Fig. 5. The fits yield to relatively high accuracy ($\pm 0.5°$) the angle, θ_D (see Fig. 6), that the principal **z** axes of **D** for $D1$ and $D2$ make with the c axis. In analyzing the data, we have made the assumption of C_{1h} symmetry, i.e., that the **y** and **z** axes lie in the $(11\bar{2}0)$ reflec-

TABLE I. Spin Hamiltonian parameters and optical dipole moment direction for the $S=1$ centers. The estimated error in the last digit(s) of each parameter is indicated in parentheses. The values of D are given in GHz. Their signs have not been determined, but the relative signs between the components of $D1$ and $D2$ are as indicated. The orientation of the relevant axes are given in Fig. 6.

	$D1$	$D2$	$D3$	$D4$	$D7$	$D8$	$D9$	$D12$
g_x	1.968(5)	1.964(5)	2.02(1)	1.962(5)	2.01(1)	2.019(2)	2.00(1)	2.015(10)
g_y	1.990(5)	2.016(5)	1.99(2)	1.980(5)	2.00(1)	2.00(1)	2.01(1)	2.02(1)
g_z	1.982(5)	1.978(5)	1.975(10)	1.972(5)	2.00(1)	2.01(1)	2.017(10)	2.00(1)
θ_g	30(10)°	14(10)°	4(10)°	14(5)°	~65°	0(10)°	~33°	~31°
D_x	±13.87(10)	∓10.83(10)	∓1.6(2)	∓4.18(2)	∓0.88(10)	±5.38(1)	∓2.28(10)	∓0.3(1)
D_y	∓13.45(10)	±10.64(10)	∓7.0(3)	±6.00(5)	∓0.90(10)	∓3.19(5)	∓2.78(10)	±2.4(1)
D_z	∓0.42(10)	±019(10)	±8.6(3)	∓1.82(5)	±1.78(10)	∓2.19(5)	±5.06(10)	∓2.1(1)
θ_D	30.0(5)°	29.7(5)°	10.1(5)°	32.4(2)°	65(2)°	0(1)°	33(1)°	31(2)°
θ_P	22(4)°	−63(10)°				90(10)°		

tion plane of the wurtzite lattice, as shown in Fig. 6. In fact, because not all of the lines can be followed throughout the full angular dependence, we cannot rule out a slight tilt of the **z** axis out of the plane, corresponding to lower, triclinic (C_1) symmetry. In order to simultaneously match the results in both planes; however, this tilt must be $\leqslant 5°$.

The relative signs given in the table for the principal values for **D** of the two spectra were estimated from the relative intensities of the high- and low-field $\Delta M_S=\pm 1$ ODEPR signals for each spectrum, as follows: In the absence of spin-lattice relaxation between the M_S states, and with $\mathbf{B}\|\mathbf{x}$, **y**, or **z**, we normally expect the intensities of the two $\Delta M_S=\pm 1$ ODEPR signals for each defect to be equal and positive, each transition always being between a pure $M_S=0$ eigenstate and a mixed $M_S=\pm 1$ one, thus taking the defect out of a state with longer radiative lifetime into a state with shorter radiative lifetime. That is not the observed case, particularly for $D2$, as can be seen in Fig. 7. One often encountered mechanism for this is if significant spin lattice relaxation occurs during the radiative lifetime of the defect. This serves to depopulate the higher-energy M_S states, which decreases (or increases) the ODEPR signal involving transitions between them and lower-energy M_S states if the higher-energy ones have the longer (or shorter) radiative lifetime. The signal with reduced amplitude will be either the higher- or lower-field transition, depending upon the sign of the fine-structure splitting. (If the spin-lattice relaxation time is shorter than the radiative lifetime, the transition will actually go negative.) If this were the sole mechanism, the sense of the asymmetry between the high- and low-field line intensities should reverse between $\mathbf{B}\|\mathbf{x}$, and **y**, because of the reversal of sign for D_x and D_y. This is not observed, the low-field transition for $D2$ remaining the weaker in both cases, as seen in the figure. This tells us that some other unknown mechanism actually dominates. Consistent with this is also the observation of no major change in the relative amplitudes vs temperature from 1.7 K to above 4.2 K. However, it is clear from the figure that the intensity *ratios* of high- to low-field lines for each defect do change by a small but significant amount for the two magnetic-field orientations, and in the opposite sense for $D1$ vs $D2$. Assuming that this can be attributed to the contribution of spin-lattice relaxation, we are led to the tentative conclusion that the signs for

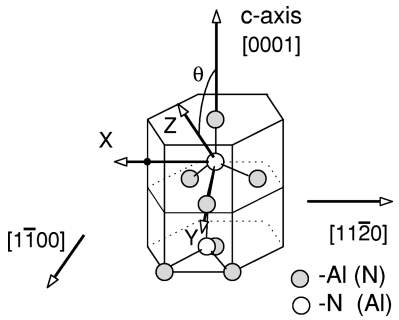

FIG. 6. AlN crystal structure. The **x**, **y**, and **z** axes shown indicate principal axes for a single defect orientation with C_{1h} symmetry. The angle θ refers to the g-tensor, θ_g, **D**-tensor, θ_D, or the optical dipole moment orientation, θ_P.

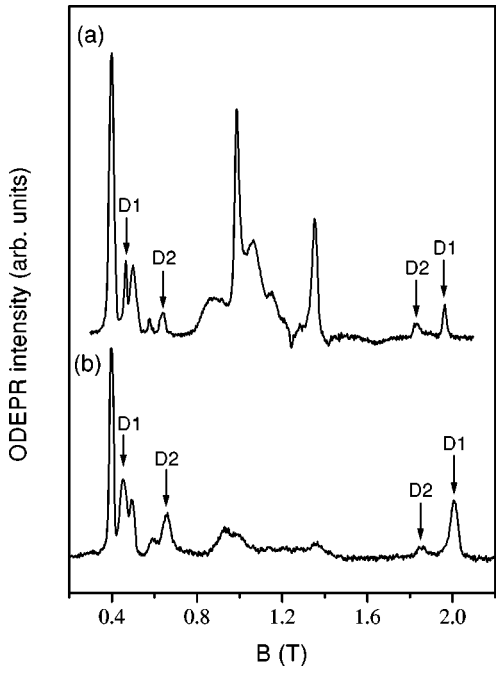

FIG. 7. (a) $D1$ and $D2$ spectra for **B** 60° away from [0001] in the (11$\bar{2}$0) plane. The two $\Delta M_S=\pm 1$ transitions for the defect with $\mathbf{B}\|\mathbf{y}$ are indicated. (b) The spectra for $\mathbf{B}\|[11\bar{2}0]$. The $\Delta M_S=\pm 1$ transitions for the defect with $\mathbf{B}\|\mathbf{x}$ are indicated.

the principal values of **D** are reversed for $D1$ and $D2$, as indicated in the table. The absolute signs cannot be determined because it has not been established which of the M_S states are the bottlenecks.

Their signals are positive and go through a maximum at a microwave modulation frequency $f_m \sim 500$ Hz, corresponding to radiative lifetimes of $\sim 330 \mu$sec.[28] However, at very low modulation frequencies, $D1$ appears to pick up negative contributions to its signals. This has been confirmed directly, where the advantage of its strong PL polarization properties (to be described in Sec. III H) allowed significant suppression of its normal signals and the corresponding signals then turned strongly negative. The spectral dependence of these negative signals reflects a broad Gaussian-shaped band shifted by ~ 0.05 eV to higher energy from that for the positive signals shown in Fig. 1. From this we can conclude that the recombination at $D1$ also serves to compete with this unrelated longer radiation lifetime band.

Earlier it was stated that the crystal surfaces were $\{1\bar{1}00\}$ planes, in analogy to SiC. Now that the relationship between the defect axes and the crystal axes has been determined, this fact can be established with certainty. In particular, since two of the principal axes of $D1$ and $D2$ must lie in (or near) a $\{11\bar{2}0\}$ plane of the crystal (the C_{1h} reflection plane), it can be concluded by noting the orientation of the sample during the experiment that the surfaces are indeed $\{1\bar{1}00\}$ planes.

B. *D*3 and *D*4

In the excitation energy dependence of Fig. 2 we see that some of the resonances that were only weakly present using the 351-nm excitation are dominant for the 458-nm excitation. These resonances are associated with two additional centers that have been labeled $D3$ and $D4$. Although they have very similar excitation wavelength dependencies, they have very different PL spectral dependencies. As shown in Fig. 1, $D3$ and $D4$ have peaks at 1.4 eV and 1.75 eV, respectively. (The data presented in the figure were obtained using a silicon detector. If, instead, a germanium detector that is sensitive to longer-wavelength light is used, it is found that $D3$ is also observed for emission from energies lower than 1.2 eV, but the ODMR signals become positive, opposite to the negative signals observed using the silicon detector.)

An angular dependence of the ODEPR signals for $D3$ and $D4$ with **B** in the $\approx(11\bar{2}0)$ plane is shown in Fig. 8. The solid lines are theoretical fits to the data using the Hamiltonian of Eq. (1) and the parameters of Table I. As was the case for $D1$ and $D2$, effective spins of $S=1$ and C_{1h} symmetry fine-structure tensors were used for both. Note that for $\Psi = 90°$, six $\Delta M_S = \pm 1$ transitions are observed for $D4$ instead of the four that are expected for a C_{1h} symmetry center with $B \| [1\bar{1}00]$. In the theoretical fit, the **B** rotation plane was taken to be tilted away from the $(11\bar{2}0)$ plane by a rotation of 3.5° around the c axis, providing an accurate fit to the data. (Because of the sample's small dimensions, there was difficulty in accurately aligning its orientation during the mounting procedure, and such a small misalignment is to be expected.) Combined with a similar angular dependence study with **B** in the $(1\bar{1}00)$ plane, the parameters given in Table I were determined.

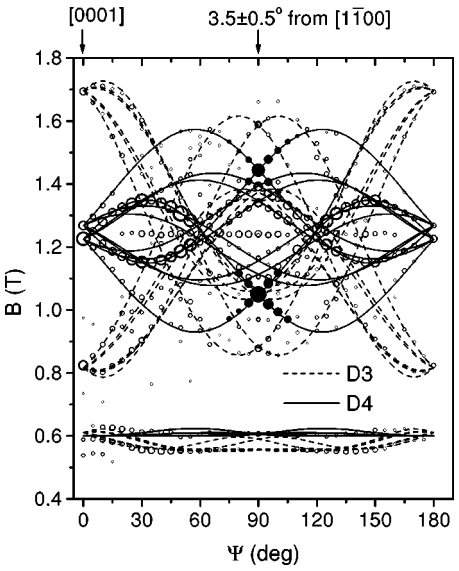

FIG. 8. Angular dependencies of $D3$ and $D4$ ODEPR signals for **B** rotated near the $(11\bar{2}0)$ plane. Open and solid circles denote negative and positive transitions, respectively. The circle areas are proportional to the ODEPR intensities. Solid ($D4$) and dashed ($D3$) lines are theoretical fits to the data using Eq. (1) and the parameters given in Table I.

The signals observed for $D3$ are negative for all orientations of **B**, suggestive of a process competing with the PL. It is unusual therefore that its spectral dependence reflects a unique PL band, as shown in Fig. 1. This suggests that it is somehow directly related to the PL band, but PL-ODEPR is detecting its spin-dependent feeding of a competing path. This competing path is presumably that being detected at longer wavelengths where its signals turn positive.

An even more curious behavior is observed for the ODEPR signals of $D4$. For a specific defect orientation the signs of its ODMR signals depend on its orientation with respect to the magnetic field. As can be seen in Fig. 2, for $B \| [1\bar{1}00]$, some defect orientations generate positive $\Delta M_S = \pm 1$ signals while others give negative signals. As discussed in the previous section, if the spin-lattice relaxation time among the M_S states is shorter than the radiative lifetime, both negative and positive ODEPR signals can occur. However, for a given orientation, the two $\Delta M_S = \pm 1$ transitions will have opposite signs. In the case of $D4$, the transitions for one orientation are both positive, while for another they are both negative, a finding that cannot be explained in terms of spin-lattice relaxation. One possible explanation is that, in this case, the center is coupled to two spin-dependent recombination paths, one of which generates the 1.75-eV band, the other not being observed. If the coupling for the two competing paths were dependent on the field orientation then the possibility would exist to observe ODEPR signals of differing signs.

C. *D*5 and *D*6

Also observed in Fig. 2 is a relatively sharp resonance near $g=2$. By reducing the modulation frequency to below

TABLE II. Spin Hamiltonian parameters for the $S=1/2$ centers. The values for A are given in MHz.

	$D5$	$D6$	$D10$	$D11$
$g_{\parallel}$	2.001(1)		1.992(1)	2.021(6)
$g_{\perp}$	2.007(1)	1.971(4)	1.992(1)	1.995(2)
$A_{\parallel}(I=5/2)$	106(2)			
$A_{\perp}(I=5/2)$	47(2)			

10 Hz, this resonance, denoted $D5$, plus another broader one at higher field, $D6$, greatly increase in intensity and become dominant, as shown on an expanded magnetic-field scale in the figure. (In fact, if one simply follows the average intensity of the luminescence, with or without microwave modulation, the intensity increase at $D5$ resonance can be as large as $\sim 1\%$, representing by far the largest contributor to the ODEPR effect in most of the WRL samples. Since we also record the total average luminescence during each PL-ODEPR magnetic-field sweep, its presence and intensity are automatically recorded even in our routine modulation frequency runs at ~ 500 Hz.) $D5$ and $D6$ have identical spectral dependencies, as shown in Fig. 1. They also have the same microwave modulation frequency and microwave power dependencies. In addition, the integrated intensities of the two resonances are equal to within 10%. All of these factors collectively suggest that these two resonances are coupled together in a long radiative lifetime distant-pair recombination process.

Angular dependence studies reveal both to be simple $S=1/2$ centers with axial symmetry around the c axis, with g values given in Table II. (Only $g_{\perp}$ could be estimated for $D6$ due to the interference from other stronger centers for $\mathbf{B}\|\mathbf{c}$ axis.) The angular dependence of $D5$ is particularly interesting, and is shown on an expanded magnetic-field scale in Fig. 9. There we show that the unusual flat-topped line shape can be simulated extremely well by including a partially resolved anisotropic hyperfine interaction

$$\mathcal{H}=\mu_B \mathbf{S}\cdot\mathbf{g}\cdot\mathbf{B}+\mathbf{I}\cdot\mathbf{A}\cdot\mathbf{S} \tag{2}$$

with a 100% abundant nucleus of $I=5/2$. The corresponding values for $\mathbf{A}$ are also included in the table.

Although the fit to $I=5/2$ is best, a reasonably satisfactory fit to the flat-topped line shape can also be made by suitably adjusting the widths of the individual m components for any 100% nucleus with I between 3/2 and 7/2. There are therefore many possibilities, including the transition element impurities ^{45}Sc,^{51}V,^{59}Co($I=7/2$), and ^{55}Mn($I=5/2$), as well as several rare earths, and normal valence impurities such as ^{9}Be,^{23}Na, etc. In addition, there is the 100% abundant ^{27}Al host atom ($I=5/2$). We cannot rule out at this stage any of the above possibilities. [Observation in the near infrared using a Ge detector revealed a sharp zero-phonon line (ZPL) at 0.8 eV, which has previously been tentatively identified with a transition-metal complex of some kind.[29] We detected no ODMR signals in it. None of the other sharp near-infrared ZPL's that have been identified with transition element impurities[29,30] were observed, however.] An argument, however, that it may be a displaced Al atom of some kind will be presented in Sec. III G, when the results of electron irradiation are described.

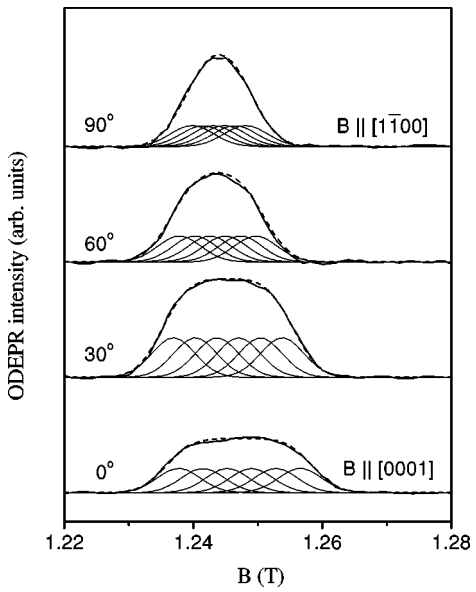

FIG. 9. Experimental line shapes of the $D5$ center (solid lines) for a few chosen orientations of the magnetic field in the $(11\bar{2}0)$ plane. The dashed lines represent theoretical fits to the data using Eq. (2) and the parameters given in Table II. Thin lines show the individual resonances for a 100% abundant nucleus of $I=5/2$.

D. $D7$

Excitation at 325 nm produces an additional signal, $D7$, shown in Fig. 2(d). Its spectral dependence is shown in Fig. 1(b). (In taking the spectrum shown in Fig. 2(d), the PL has been passed through a 2.5-eV high-energy pass filter to suppress the other signals for clarity.) The signals are only partially resolved, but angular dependent studies in both the $(1\bar{1}00)$ and (0001) planes provide the tentative analysis as a $C_{1h}S=1$ center, with the Eq. (1) spin Hamiltonian parameters given in Table I.

Also evident in the spectrum of Fig. 2, is the presence of a negative signal in the center at $g\approx 2$. It becomes stronger at lower modulation frequencies and appears closely isotropic. Since it has no clearly distinguishing features, it will not be considered further. We cannot rule out, e.g., that it is $D5$.

E. $D8$, $D9$, and $D12$

In the GERL samples, three distinct new $S=1$ ODEPR signals are observed, as shown in Fig. 4. Their signal intensities maximize at $f_m\sim$ 100–200 Hz, indicating radiative lifetimes ~ 1 ms,[28] somewhat longer than $D1$–$D4$. Labeled $D8$, $D9$, and $D12$, their spectral dependencies are shown in Fig. 3. $D8$ can be conveniently isolated by excitation at 458 nm, with a suitable high pass filter, as shown in Fig. 4(d), and studies of its angular dependence in the $(1\bar{1}00)$ and (0001) planes gives the spin Hamiltonian parameters in Table I. $D12$ can also be conveniently isolated by appropriate filtering, as shown in Fig. 4(c), but its small fine-structure splitting compared to the breadth of its lines makes

its analysis in Table I only tentative. $D9$ is not so easily separated, and its analysis in Table I, which accounts satisfactorily for the those of its transitions that can be accurately followed, must still be considered, also, only as tentative. All of the signals are positive in their respective bands. The $D8$ signals are observed to turn negative at very low modulation frequencies, but spectral dependence studies reflect a band shifted to higher energy by ~ 0.020 eV, with which the $D8$ direct (positive) spin-dependent luminescence process is competing.

F. $D10$ and $D11$

In the GERL samples, two sharp axially symmetric $g \simeq 2$, $S=1/2$ centers are observed, as seen on an expanded magnetic-field scale, in Fig. 4(b). Their spectral dependencies are identical, as shown in Fig. 3, and their g values are included in Table II. Their intensities are optimized at higher modulation frequencies, ~ 1 kHz, indicating a shorter radiative lifetime.

G. Effect of electron irradiation

Electron irradiation supplies a convenient method to displace lattice atoms and produce intrinsic vacancy and interstitial point defects. We have initiated such studies on a few of these samples and report here briefly our preliminary results.

One as-grown sample of the WRL samples was found to display $D1$–$D4$ but $D5$ was absent. It was subsequently irradiated at room temperature by 2.5 MeV electrons in three stages to total doses of 0.5, 1.0, and 2×10^{18} cm^{-2}. There was little change in the luminescence and in the strength of the $D1$–$D4$ spectra. However, the $D5$ spectrum emerged strongly after the 1.0×10^{18} cm^{-2} dose, and doubled to a strength comparable to that in the other samples after the last irradiation. This suggests that the $D5$ defect may be being produced by the irradiation and therefore related to a primary defect, i.e., a vacancy or interstitial. If so, this supplies a strong argument for identifying its $I=5/2$ hyperfine interaction with ^{27}Al. This might arise, for example, from an isolated or trapped interstitial Al atom, or N vacancy, with the unpaired electron in the latter case strongly localized on its c axis Al near neighbor.

A GERL sample was similarly irradiated. For it, the PL intensity was strongly reduced (factor of ~ 5–10) after a first dose of 1×10^{18} cm^{-2}, and, as shown in Fig. 10, it sharpens somewhat as its lower-energy tail disappears. Subsequent irradiation produces little further change. In the PL-ODEPR, after the first irradiation, $D9$, $D8$, and $D12$ remained with comparable intensity to the before radiation results, but $D10$ and $D11$ disappeared completely. The disappearance of $D10$ and $D11$ explains nicely the change in intensity and shape of the PL, as shown by comparing Fig. 10 to Fig. 3, revealing that $D10$ and $D11$ produce the major component of the PL in the as-grown state of the GERL samples. In the subsequent irradiations, the strength of the negative $D8$ signals seen at low modulation frequency increases, suggesting an increase in the concentration of defects with which it is competing.

Neither $D5$ or any other prominent new ODEPR signals have been detected so far in the electron-irradiated GERL sample.

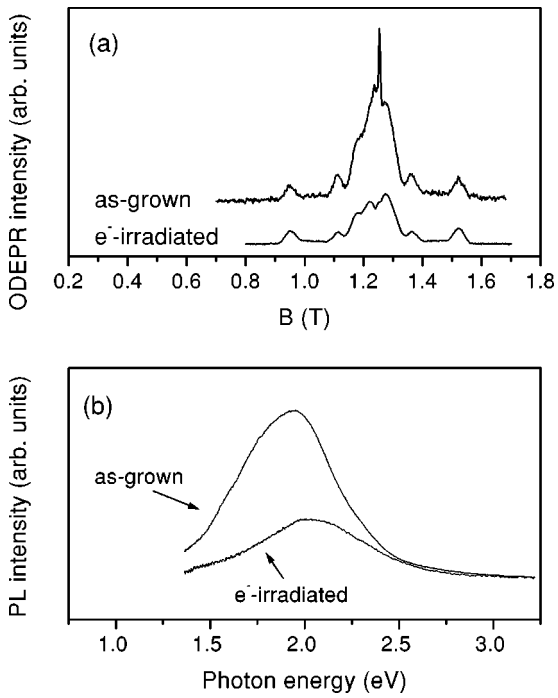

FIG. 10. Comparison of ODEPR (a) and PL (b) spectra in an as-grown and electron-irradiated GERL sample.

H. Polarization properties

The luminescence of each of the crystals was found to display preferential polarization properties with respect to its c axis. The degree of polarization was observed to depend upon the emission wavelength, and the polarization and energy of the exciting light. Measurement of the polarization properties of the individual PL-ODEPR signals provides a powerful way of helping to unravel the various processes involved: For each ODEPR spectrum, the different component lines arise from different equivalent orientations of the corresponding defect with respect to the magnetic field. By placing a polarizer in the collected PL beam (emitted along the magnetic field), the direction of the polarization vector component in the plane perpendicular to the collection direction can be determined for each defect orientation by the intensity of its signal. In such a study, the effect of direction and polarization of the exciting light can also be studied.

No evidence of circular polarization was found in the emission for any of the centers. However, there is clear evidence that one of the $S=1/2$ centers, $D5$, and all of the $S=1$ centers, with the exception of $D12$, display linear polarization properties in emission, and, in some cases, polarized excitation properties, as well. We have performed detailed studies of these properties for four of the more prominent centers, $D1$, $D2$, $D8$, and $D5$, the results of which we now briefly describe.

In Fig. 11, the strong linear polarization effects for the PL of $D1$ and $D2$ are illustrated. Here, with the polarization vector $\mathbf{E}\|[0001]$, the lines, labeled (a), arising from the defect orientation for which $\mathbf{B}$ is parallel to its $\mathbf{x}$-axis have full strength for $D1$, but are very weak for $D2$. Conversely, for $\mathbf{E}\|[1\bar{1}00]$, the corresponding lines for $D2$ have full intensity, and for $D1$ they are weak. The other lines of each, labeled (b), which correspond to differently oriented defects,

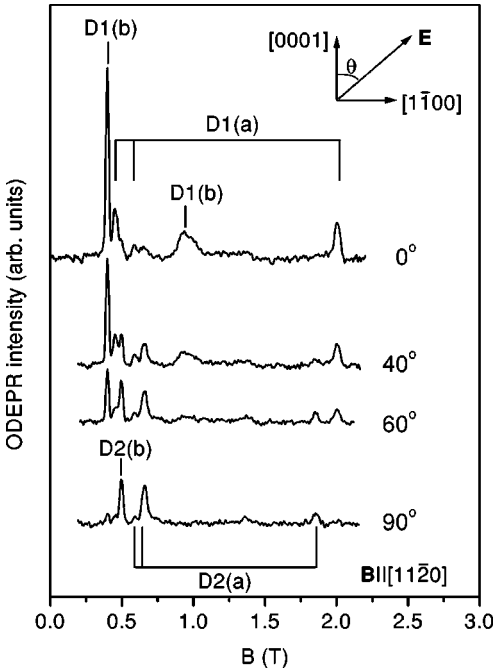

FIG. 11. ODEPR spectra of $D1$ and $D2$ for $\mathbf{B}\|[11\bar{2}0]$ recorded with a linear polarizer placed in front of the detector. The polarizer axis was rotated in the $(11\bar{2}0)$ plane, as shown in the figure. Two different orientations of $D1$ and $D2$ are indicated. The ones labeled (a) have their **y** and **z** axes in the polarization plane, the principal axes for orientations (b) are out of the plane. The spectra were taken with a high-energy pass filter to suppress $D3$ and $D4$.

also display strong, but different, polarization properties. With the collection geometry shown in the figure, a detailed study of the intensity of the ODEPR lines vs the angular orientation of the polarizer was performed, as shown. The intensity for the ith defect orientation was analyzed as $\sim(\mathbf{E}\cdot\mathbf{P}_i)^2$, where $\mathbf{P}_i$ is the optical dipole transition moment vector for the defect. Combined with similar studies for $\mathbf{B}\|[1\bar{1}00]$, $\mathbf{P}_i$ for $D1$ was established to be in the C_{1h} **y**-**z** reflection plane with the angle $\theta_P=22\pm4°$, as shown in Fig. 6, and listed in Table I. $D2$ was determined to be polarized also in this plane, with $\theta_P=-63\pm10°$, i.e., essentially perpendicular to that of $D1$.

(The strong PL anisotropy for $D1$ was taken advantage of in the study described in Sec. III A. By orienting the polarizer to accept only PL perpendicular to the C_{1h} reflection plane of one set of the defects, the direct ODEPR signals from them could be eliminated. At low modulation frequencies the signals reemerged, but negative, reflecting a different band with which the spin-dependent $D1$ process was competing.)

A similar study for $D8$, revealed the PL polarization vector also to be in the defect C_{1h} reflection plane (the **y**-**z** plane) but perpendicular to the c-axis (i.e., parallel to the defect **y** axis, with $\theta_P=90\pm10°$). Surprisingly, however, the rather distinct PL band associated with $D8$ appeared to display a $\approx2:1$ preferential polarization *along the c axis*. This suggests that there may be an additional closely related emission band associated with the defect but for which ODEPR is not detected. It could, for example, involve emission from an energetically close singlet state.

The intensity of the $D8$ ODEPR signals also showed strong dependence on the polarization of the excitation when excited with the 458-nm laser line. For higher-energy excitation, the effects were greatly reduced. We interpret this to indicate that the defect is excited directly by the 458-nm excitation. A preliminary study indicates the excitation polarization to be in the C_{1h} reflection plane of the defect, but without large variation within the plane. (An absorption band centered at ~2.76 eV has previously been reported for the specific W-154 sample studied here,[26] suggesting a possible connection with $D8$.)

The emission polarization properties of $D5$ reveal themselves in a dependence of the relative intensity of its parallel and perpendicular emission components on the polarization of the excitation. For example, with 351-nm excitation parallel to the c axis, the ODEPR signal in the parallel emission component exceeds that in the perpendicular component by 2:1. For equal parallel and perpendicular excitation (circularly polarized by insertion of a 1/4 wave plate), the ratio is reduced to $\approx1.3:1$.

IV. DISCUSSION

We have demonstrated that single crystals of AlN can be very rich in their ODEPR spectra. This is a welcome discovery when noting the paucity of such interesting spectra in its sister wide bandgap semiconductor GaN.[31–34] With the discovery of this plethora of strong, distinct, well-resolved, anisotropic ODEPR spectra the possibility becomes more promising that we may finally now be able to begin to unravel and understand defects in the technologically important III-V nitrides through the window provided by this material. At present, however, it is still only *promising.* All except one of the spectra, $D5$, display no resolved hyperfine structure to help identify the chemical constituents of the defects. We now consider $D5$ in more detail, as well as $D1$ and $D2$, around which a major part of our study has centered.

A. $D5$

This $S=1/2$ center is the only one to display hyperfine interaction, and, as a result, contain chemical information concerning its constituents. As mentioned in Sec. III C, hyperfine interaction with any 100% abundant $I=3/2$, 5/2, or 7/2 nucleus is a possibility. Optical detection of electron-nuclear double resonance (ODENDOR) could potentially determine the nuclear magnetic moment and spin of the nucleus, providing the necessary identification. However, preliminary ODENDOR attempts have so far been unsuccessful. They will be continued, but, in the meantime, let us consider the intriguing possibility that it is a displaced aluminum host atom of some kind.

We can compare estimates of the ^{27}Al free neutral atom hyperfine interactions for a $3s(a=2747$ MHz) and $3p(b=60.6$ MHz) orbital[35] to the observed values of $|A_\||=|a+2b|=106\pm2$ MHz and $|A_\perp|=|a-b|=47\pm2$ MHz. This gives, for the required fractional components of the wavefunction on the aluminum atom, 33% $3p$ and 2.4% $3s$, or 84% $3p$ and negligible $3s$, depending upon whether $A_\|$ and $A_\perp$ have the same signs, or opposite, respectively. In

either case these are reasonable values representing a high degree of localization in a *p*-orbital pointing along the *c* axis of the crystal.

The fact that $D5$ was produced by electron irradiation in a WRL sample in which it was originally absent is clearly also consistent with its identification with a displaced Al atom of some kind. However, the failure to produce it in the presumably purer GERL samples makes the argument less convincing. The problem is, of course, that under optical excitation at cryogenic temperatures, and with such a wide-band-gap material, it is difficult to interpret the presence or absence of a particular luminescence process to indicate the presence or absence of the responsible defect. The concept of a Fermi level has no relevance, and the charge states of defects and their relative roles in competing radiative and nonradiative processes depend in a complicated way on the relative concentration of the individual defects, their electron and hole capture cross sections, etc. Hopefully, we will be able to begin to partially sort these questions out as these studies are continued.

In the meantime, we tentatively conclude that the weight of the evidence favors a displaced aluminum atom of some kind. It could be an interstitial Al atom, or a N vacancy with the unpaired electron located primarily on the *c*-axis aluminum neighbor. And it could be either isolated or, more likely, trapped by some other impurity or defect. The fact that, when detected, it is accompanied by another positive, equal integrated intensity $S=1/2$ center, $D6$, suggests that the mechanism for their detection is spin-dependent recombination luminescence between the two.

B. $D1$ and $D2$

$D1$ and $D2$, like all of the remaining centers, display no resolved hyperfine interactions. We have no clue, therefore, as to their chemical constituents. However, they do display some intriguing properties, which we now explore.

They always appear together, and display almost identical spectral dependencies. They both have C_{1h} symmetry with a near-zero principal value for **D** along a direction $\sim 30°$ from the *c* axis in the C_{1h} reflection plane. The magnitudes of their *D*-value components along the other two principal axes are similar, but their signs appear to be reversed. The PL polarization vectors for the two are both in the C_{1h} reflection plane, but approximately perpendicular to each other.

These properties suggest that the two are associated with the same defect, representing PL from two different, but energetically closely spaced, excited states. We now describe two possible models that we have considered.

1. Model A

The unusual dihedral symmetry for **D**, and the reversed signs for the components of the two suggests a very simple model: Consider the excited emitting states to be the $S=1$ combinations of a spatially separated electron and hole, with the fine-structure tensors **D** arising from magnetic dipole-dipole interaction between them. For the unique case of one of the particles being spread equally between two sites at a distance *r* from the other particle, and making the tetrahedral angle of 109.4° between them as viewed from the other particle, the principal *D*-tensor components become simply[36]

$$D_\alpha = -D_\beta = \frac{\mu_0}{8\pi} g_e g_h \mu_B^2 \frac{1}{r^3} \tag{3}$$

and

$$D_\gamma = 0. \tag{4}$$

Here the γ axis bisects the angle between the two separated sites, and the α axis is perpendicular to the plane of the particles.

This is just what one expects for one particle located at a lattice site and the other spread equally between two of its nearest neighbors. There are two possibilities: (a) one of the split particles is on the *c*-axis neighbor, or (b) neither is on the *c*-axis neighbor. Both have C_{1h} symmetry but the α and β axes are interchanged, accounting for the reversal in signs for the *x* and *y* components of *D* for $D1$ and $D2$. With Eq. (3), the magnitudes of D_x and D_y give $r=1.23$ Å for $D1$ and 1.34 Å for $D2$. Compared to the nearest-neighbor distances in AlN of 1.86 Å and 1.90 Å,[37] these are significantly smaller, but not out of the question, perhaps, for an average $\langle 1/r^3 \rangle$ between extended atomic orbitals on the atoms.

There is a serious problem, however, with this otherwise attractively simple and successful model for the two excited states of the defect. It is the orientation of the *z* axis. For the undistorted lattice the bisector to two adjacent sites makes an angle of $\sim 55°$ to the *c* axis, not 30°. In addition, the approximately perpendicular polarization properties of $D1$ and $D2$ do not appear to arise in an obvious fashion from the model. And so it must be somewhat more complicated than this. It is possible, for example, that a significant rearrangement of the local atom sites involved has occurred at the defect. For example, theoretical calculations predict large lattice relaxations for interstitials in the similar GaN wurtzite lattice.[38] In another theoretical study, large $(\sim 1\text{Å})c$-axis displacements have been predicted for oxygen on a N site in AlN, accompanying *DX*-like behavior.[39] In addition, the breadth of the luminescence band provides strong evidence of significant lattice relaxations occurring during the transition. Or, alternatively, the defect might even be a separate molecular unit with tetrahedral bonding that has been incorporated, appropriately tilted, into the lattice, and it is its similar intramolecular excitations that are being observed. For example, molecular units involving two or more oxygen atoms bonded to an impurity suggest themselves.

In any event, the fact that dipole-dipole interaction between two particles that are displaced symmetrically in two tetrahedral directions uniquely produces the unusual dihedral symmetry for **D**, and at the same time provides for the two sign possibilities, makes this model difficult to discard.

2. Model B

We have also briefly considered the possibility that the emission is from a bound exciton, with a shallow effective mass hole and a deeply bound electron. In that case the two excited states could arise from the binding of one or the other of the two valence-band hole states which are split by the wurtzite crystal field. The polarization properties could then reflect primarily those of the two *p*-like hole states (one pointing along the *c* axis, the other made up from the two perpendicular to the *c* axis), explaining in part, the orthogo-

nal polarization relations between $D1$ and $D2$. In this case, however, we might expect significant orbital contributions to the g values from the perpendicular p-oriented hole states, which are not seen in either $D1$ or $D2$. Also, dipole-dipole interactions would be too weak to explain the fine-structure terms and it would be necessary to consider spin-orbit mixing from higher-lying excited states. Assuming, therefore, that the orbital contribution to the perpendicular p-orbital state is somehow quenched, perhaps by the low local symmetry of the defect, we can then explore the possibility of this mechanism further.

Spin-orbit interaction with excited states also causes an anisotropic departure of the g value from the free-electron value of 2.0023. In the case of an orbital singlet ground state, the following relationship exists between the g and D tensors,[36]

$$\frac{1}{2}\Delta\mathbf{g}\cdot\lambda=\mathbf{D}, \tag{5}$$

where

$$\Delta\mathbf{g}=\mathbf{g}-2.0023. \tag{6}$$

Selecting the larger of the two atomic spin-orbit parameters ($\lambda=9.2$ meV for ^{27}Al, 5.6 meV for ^{14}N),[40] the experimental anisotropy $g_z-g_x=0.014$ for both $D1$ and $D2$ predicts, with Eq. (5), a magnitude for D_z-D_x of 16 GHz. So, the observed magnitude (14 GHz for $D1$) could possibly be accounted for. However, the sign of the g anisotropy for $D14$ and $D2$ is the same, while the D anisotropy is reversed. Therefore, this model, by itself, must be discarded.

We conclude therefore that some variation of model A represents the best choice at this stage. Perhaps, introducing some of the concepts of model B into model A will help. In particular, the experimental g anisotropy implies some contribution from spin-orbit mixing, and therefore possibly nonnegligible contributions to **D**. Therefore, taking account, in model A, of preferential orientation for the localized p-orbital holes in the two states might provide net tilts for the D_z axes and significant contributions to the polarization properties of the defects, which are not directly accounted for otherwise in the model. At the same time, it could retain the major dihedral contributions to **D** from the magnetic dipole-dipole interactions, which reflect primarily the *spatial* locations of the particles.

3. The other centers

The two $S=1/2$ centers in the GERL samples, $D10$ and $D11$, share the same spectral dependence. Like $D5$ and $D6$, therefore, they are most probably being observed via spin-dependent recombination luminescence between the two. Each of the other $S=1$ centers, with the exception of $D12$, shows distinct polarization properties of the emitted PL for its differently oriented defects. Therefore, as for $D1$ and $D2$, it can be concluded that, for each of them, the luminescence comes directly from the decay of the excited $S=1$ state seen in its PL-ODEPR.

V. SUMMARY

In contrast to GaN,[31–34] this study suggests that AlN can be expected to be rich in centers accessible to the PL-ODEPR technique. As-grown impurities present in single-crystal AlN have been shown to produce a variety of luminescent centers in the visible and near-infrared regions. Several $S=1$ centers ($D1$, $D2$, $D3$, $D4$, $D7$, $D8$, $D9$, $D12$) and distant $S=1/2$ pair recombinations ($D5$ with $D6$, $D10$ with $D11$) have been observed in these bands via ODEPR. In all except one, no resolvable hyperfine interactions have been observed, and the important chemical information that they provide is missing. This can at least be partially explained by the low abundance of nuclei with nuclear spins for the primary suspected chemical impurities, oxygen and carbon, as well as for many of the commonly suspected transition element impurities, such as titanium, chromium, iron, and nickel.

The $S=1/2$ center $D5$ displays an anisotropic flat-topped shape that can be matched well by an anisotropic hyperfine interaction with a 100% abundant nucleus of $7/2\geqslant I\geqslant 3/2$. We have presented arguments to identify the nucleus as ^{27}Al, and therefore associated with a displaced host aluminum atom of some kind. Tentatively consistent with this identification, the center is produced by 2.5 MeV electron irradiation in a sample for which the signal was initially absent. Two of the $S=1$ centers, $D1$ and $D2$, appear to arise from two energetically closely spaced excited states of a single defect. A simple model of spatially separated electron and hole among neighbor atom sites can provide an explanation for the unusual dihedral form of **D** for both, and their apparent opposite sign. In its simplest form, however, it has problems in predicting accurately the orientation of **D** or certain features of the PL polarization properties. Possible improvements to the model include orbital effects for the bound holes, as well as significant lattice relaxations of the involved atoms.

ACKNOWLEDGMENTS

The research was supported jointly by the U.S. Navy Office of Research (Electronics and Solid State Sciences Program) under Grant No. N00014-94-1-0117, and the National Science Foundation under Grants No. DMR-92-04114 and DMR-97-04386.

*Present address: Lucent Technologies, 9333 S. John Young Pkwy, Orlando, FL 32819.

†Present address: Institute of Physics, Polish Academy of Sciences, Warsaw, Poland.

[1] S. Strite, M. E. Lin, and H. Morkoç, Thin Solid Films **231**, 197 (1993).

[2] S. Strite and H. Morkoç, J. Vac. Sci. Technol. B **104**, 1237 (1992).

[3] H. Morkoç, Mater. Sci. Forum **239-241**, 119 (1997).

[4] R. F. Davis, Proc. IEEE **79**, 702 (1991).

[5] G. A. Slack, R. A. Tanzilli, R. O. Pohl, and J. W. Vandersande, J. Phys. Chem. Solids **48**, 641 (1987).

[6] S. Pacesova and L. Jastrabik, Czech. J. Phys., Sect. B **29**, 913 (1979).

[7] R. A. Youngman and J. H. Harris, J. Am. Ceram. Soc. **73**, 3238 (1990).

[8] G. E. Archangelskii, M. V. Fock, S. I. Pacesova, and L. Jastrabik, Phys. Status Solidi B **108**, K117 (1981).
[9] F. Karel, J. Pastrnak, J. Hejduk, and V. Losik, Phys. Status Solidi **15**, 693 (1966).
[10] F. Karel and J. Pastrnak, Czech. J. Phys., Sect. B **20**, 46 (1970).
[11] J. Baur, K. Maier, M. Kunzer, U. Kaufmann, and J. Schneider, Appl. Phys. Lett. **65**, 2211 (1994).
[12] J. Baur, U. Kaufmann, M. Kunzer, J. Schneider, H. Amano, I. Akasaki, T. Detchprohm, and K. Hiramatsu, Appl. Phys. Lett. **67**, 1140 (1995).
[13] K. Pressel, R. Heitz, S. Nilsson, P. Thurian, A. Hoffmann, and B. K. Meyer, in *Gallium Nitride and Related Materials*, edited by F. A. Ponce, R. D. Dupuis, S. Nakamura, and J. A. Edmond, MRS Symposia Proceedings No. 395 (Materials Research Society, Pittsburgh, 1996), p. 613.
[14] P. Thurian, I. Loa, P. Maxim, K. Pressel, A. Hoffmann, and C. Thomsen, Mater. Sci. Forum **258-263**, 1131 (1997).
[15] J. Baur, K. Maier, M. Kunzer, U. Kaufmann, J. Schneider, H. Amano, I. Asaki, T. Detchprohm, and K. Hiramatsu, Appl. Phys. Lett. **64**, 857 (1994).
[16] R. Heitz, P. Thurian, I. Loa, L. Eckey, A. Hoffmann, I. Broser, K. Pressel, B. K. Meyer, and E. N. Mokhov, Appl. Phys. Lett. **67**, 2822 (1995).
[17] R. Heitz, P. Thurian, I. Loa, L. Eckey, A. Hoffmann, I. Broser, K. Pressel, B. K. Meyer, and E. N. Mokhov, Phys. Rev. B **52**, 16 508 (1995).
[18] K. Atobe, M. Honda, N. Fukuoka, M. Okada, and M. Nakagawa, Jpn. J. Appl. Phys., Part 1 **29**, 150 (1990).
[19] M. Honda, K. Atobe, N. Fukuoka, M. Okada, and M. Nakagawa, Jpn. J. Appl. Phys., Part 2 **29**, L652 (1990).
[20] T. L. Tansley and R. J. Egan, Phys. Rev. B **45**, 10 942 (1992).
[21] D. W. Jenkins, J. D. Dow, and M. Tsai, J. Appl. Phys. **72**, 4130 (1992).
[22] P. Boguslawski, E. Briggs, T. A. White, M. G. Wensell, and J. Bernholc, in *Diamond, SiC, and Nitride Wide Bandgap Semiconductors*, edited by C. H. Carter, Jr., G. Gildenblat, S. Nakamura, and R. J. Nemanich, MRS Symposia Proceedings No. 339 (Materials Research Society, Pittsburgh 1994), p. 693.
[23] T. Mattila and R. M. Nieminen, Phys. Rev. B **54**, 16 676 (1996).
[24] R. B. Campbell and H. C. Chang, in *Solid State Ultrasonic Devices for Fire Detection in Advanced Flight Vehicles* (National Technical Information Services Clearinghouse, Springfield, VA, 1967).
[25] R. W. Keyes, in *SiC*, edited by I. R. O'Connor and J. Smiltens (Pergamon, New York, 1960), p. 217.
[26] G. A. Slack and T. F. McNelly, J. Cryst. Growth **42**, 560 (1977).
[27] M. H. Nazare, P. W. Mason, G. D. Watkins, and H. Kanda, Phys. Rev. B **51**, 16 741 (1995).
[28] W. A. Barry and G. D. Watkins, Phys. Rev. B **54**, 7789 (1996).
[29] K. Pressel, R. Heitz, S. Nilsson, P. Thurian, A. Hoffmann, and B. K. Meyer, in *Gallium Nitride and Related Materials*, edited by F. A. Ponce, R. D. Dupuis, S. Nakamura, and J. A. Edmond, MRS Symposia Proceedings No. 395 (Materials Research Society, Pittsburgh, 1996), p. 613.
[30] J. Baur, U. Kaufmann, M. Kunzer, J. Schneider, H. Amano, I. Asaki, T. Detchprohm, and K. Hiramatsu, Mater. Sci. Forum **196-201**, 55 (1995).
[31] E. R. Glaser, T. A. Kennedy, K. Doverspike, L. B. Rowland, D. K. Gaskill, J. A. Frietas, Jr., M. Asif Khan, D. T. Olson, J. N. Kunzia, and D. K. Wickenden, Phys. Rev. B **51**, 13 326 (1995).
[32] F. K. Koschnick, J. M. Spaeth, E. R. Glaser, K. Doverspike, L. B. Rowland, D. K. Gaskill, and D. K. Wickenden, Mater. Sci. Forum **196-201**, 37 (1995).
[33] U. Kaufmann, M. Kunzer, C. Merz, I. Akasaki, and H. Amano, in *Gallium Nitride and Related Materials*, edited by F. A. Ponce, R. D. Dupuis, S. Nakamura, and J. A. Edmond, MRS Symposia Proceedings No. 395 (Materials Research Society, Pittsburgh, 1996), p. 633.
[34] D. M. Hofmann, D. Kovalev, G. Steude, B. K. Meyer, A. Hoffmann, L. Eckey, R. Heitz, T. Detchprohm, H. Amano, and I. Akasaki, Phys. Rev. B **52**, 16 702 (1995).
[35] A. K. Koh and D. J. Miller, At. Data Nucl. Data Tables **33**, 235 (1985).
[36] J. A. Weil, J. R. Bolton, and J. E. Wertz, *Electron Paramagnetic Resonance, Elementary Theory and Practical Applications* (Wiley, New York, 1994).
[37] W. G. Wyckoff, *Crystal Structures* (Wiley, New York, 1963), p. 112.
[38] P. Boguslawski, E. L. Briggs, and J. Bernholc, Phys. Rev. B **51**, 17 255 (1995).
[39] C. C. Van de Walle, Phys. Rev. B **57**, 2033 (1998).
[40] Approximated using the Landé interval rule, $J(n)\lambda = E_n - E_{n-1}$, using values listed in *Atomic Energy Levels*, edited by C. E. Moore, Natl. Bur. Stand. Ref. Data Ser., Natl. Bur. Stand. (U.S.) Circ. No. 467 (U.S. GPO, Washington, D.C., 1949).